

Optimized templates for bottom-up growth of high-performance integrated biomolecular detectors

Cite this: *Lab Chip*, 2013, 13, 2569

Brian Lam,^a Richard D. Holmes,^b Jagotamoy Das,^c Mahla Poudineh,^d Andrew Sage,^c Edward H. Sargent^d and Shana O. Kelley^{*abcde}

Electrochemical deposition of metals represents an important approach in the bottom-up fabrication of nanostructures and microstructures. We have used this approach to generate high-performance chip-based biosensors using silicon as a platform for the generation of sensor arrays. Here, we explore the applicability of different materials to support the electrodeposition and identify the parameters that are essential for robust sensor growth. We show that inexpensive materials can be used as templates for electrodeposition, and demonstrate that these low-cost sensors exhibit clinically-relevant levels of sensitivity and specificity. In particular, we prove herein that the glass-based sensors successfully detect *E. coli* in urine, when present at the 100 cfu μL^{-1} levels found typically in samples of patients with urinary tract infections.

Received 24th December 2012,
Accepted 7th February 2013

DOI: 10.1039/c3lc41416g

www.rsc.org/loc

Introduction

Chip-based biosensors are an important class of tools for integrated biomolecular detection devices, and enable specific identification of clinically-relevant biomarkers.^{1–8} Sensors that read out protein, nucleic acid or small molecular biomarkers can be used to classify disease states or monitor progression. A variety of readout methods have been used in conjunction with chip-based sensors, including colorimetric,^{7,9} fluorescence,^{3,10} electronic^{8,11} and electrochemical approaches.^{4,12–17}

A key limitation of chip-based sensors relates to efficient capture of molecular analytes.^{18–20} Generating a detectable signal requires a collision between a molecule of interest and a sensor that is able to capture and detect the molecule. Unfortunately, collisional frequencies achieved with planar sensors can be low. We recently reported a solution to this limitation, one that relies on the fabrication of microscale three-dimensional electrodeposited structures sensors that enable efficient capture and readout of slow-moving mRNA molecules.²¹ Electrodeposition is one of the few approaches available that permits the production of large (>50 micron) structures that are three-dimensional, and has the added advantage of producing tunable surface morphology at the

nanoscale.^{22–23} We have used these features of nanostructured microelectrodes (NMEs) to control dynamic range, and have also shown that a combination of structural features on the nano- and microscale are essential for attaining clinically-relevant levels of sensitivity.^{21,22}

Templated electrodeposition is widely used in the generation of nanostructured surfaces, nanowires, and nanoparticles, and its tunability has been exploited to tailor the sizes and shapes of these nanomaterials.^{24–29} Less work has been done, however, on the growth of three-dimensional microscale structures that are produced using this technique. The properties of the base substrate, the material used for templating, and the size and shape of the aperture used as a template could all have an effect on the resultant structure and its performance. Our previous work leveraged electrodeposition to produce nanostructured microelectrodes-structures composed of gold or palladium that were coated with a nanostructured layer of palladium. In prior studies, we explored how nanostructuring and sensor size affect sensor performance, but did not investigate the tolerance of the approach to different chip structures and substrates.^{16,21–23} Here, we investigate a variety of materials – including glass, plastic and printed circuit board as substrates – and evaluate their performance. We identify the critical features that a material must have to support the electrodeposition of microscale structures. Using low-cost-substrates identified during this study, we demonstrate that high levels of sensitivity and specificity are maintained by the sensors, and we explore the relationship between template properties and sensor morphology.

^aDepartment of Chemistry, Faculty of Arts and Sciences, University of Toronto, Toronto, ON, Canada M5S 3M2. E-mail: shana.kelley@utoronto.ca

^bInstitute of Biomedical and Biomaterials Engineering, Faculty of Engineering, University of Toronto, Toronto, ON, Canada M5S 3M2

^cDepartment of Pharmaceutical Science, Leslie Dan Faculty of Pharmacy, University of Toronto, Toronto, ON, Canada M5S 3M2

^dDepartment of Electrical and Computer Engineering, Faculty of Engineering, University of Toronto, Toronto, ON, Canada M5S 3M2

^eDepartment of Biochemistry, Faculty of Medicine, University of Toronto, Toronto, ON, Canada M5S 3M2

Materials and methods

A. Silicon chip fabrication

Chips were fabricated by Advanced Micro Sensors (Shrewsbury, MA) on the surface of 6" diameter 300 μm thick prime silicon wafers obtained from Silicon Valley Microelectronics (Santa Clara, CA). Wafers were first passivated with a 1 μm layer of thermal SiO_2 to isolate the sensing electrodes. Using positive photoresist a lift-off layer was patterned on the surface of the oxide. A metal layer consisting of 5 nm Ti followed by 50 nm Au was evaporated onto the surface, followed by lift-off to create the sensing electrode layer. A SiO_2 passivating layer was deposited on the surface using Plasma Enhanced Chemical Vapor Deposition. Using positive photoresist an aperture etch mask was patterned on the surface and 5 μm apertures were etched into the SiO_2 layer using hydrofluoric acid. Fabrication of nanostructured microelectrodes (NMEs) on the surface was done by electroplating in a solution of 20 mM HAuCl_4 and 0.5 M HCl at a constant potential of 0 mV for 90 s. A finely nanostructured Pd coating was electroplated by using a solution of 5 mM PdCl_2 and 0.5 M HClO_4 at a constant potential of -250 mV for 10 s.

B. Printed circuit board chip and nme fabrication

PCB chips were fabricated by Omega Circuits (Toronto, ON) on the surface of standard FR-4 fiberglass board. Boards were pre-coated with copper foil. A shadowmask is first laminated onto the surface of the board and patterned in similar fashion to positive photolithography, but achieving less fine resolution (e.g. typical critical dimensions on the 10–20 μm lengthscale). Boards are immersed in a copper etchant to create the sensing electrode layer. Soldermask is applied to the surface of the board, and acts as an aperture layer similar to the silicon chips. The soldermask is patterned in a similar fashion to negative photoresist and apertures ~ 40 μm in diameter were created in the aperture layer. Individual PCB chips are machined from the board using an auto router. Corrosion of the Cu layer immediately occurs in above plating solution. An alternative plating method utilizes a Ni protection layer from electroplating in 200 mM NiSO_4 and 0.5 M HBO_3 at -850 mV for 1 h followed by an Au electrode layer from electroplating in 20 mM HAuCl_4 and 0.5 M NaOH at -400 mV for 60 s. A second alternative method utilized a Au sulfite protection layer by electroplating in a gold sulfite solution obtained from Transene Inc (Danvers, MA) at -500 mV for 1 h followed by an Au electrode layer from electroplating in 20 mM HAuCl_4 and 0.5 M HCl at 0 mV for 90 s.

C. Plastic chip and nme fabrication

Plastic chips were fabricated by MiniFAB (Scoresby, AUS) on the surface of fluorinated ethylene polymer (FEP) film. Sensing electrodes were printed on the surface of the film using a colloidal gold ink. Chips were made on flexible FEP film which is not suitable for spin coating, hence we first adhered them to glass to act as a rigid substrate. We spun a negative photoresist SU-8 3005 (3000 rpm, 30 s) to create the aperture layer, which is patterned using contact lithography to create apertures ~ 40 μm in diameter. Better resolution was not achievable because the substrate is not perfectly rigid and the contact of the mask

to the surface is not optimal. Fabrication of NMEs on the surface was done by electroplating in a solution of 20 mM HAuCl_4 and 0.5 M HCl at a constant potential of 0 mV for 90 s.

D. Glass chip fabrication

Glass chips were fabricated in-house utilizing substrates obtained from Telic Company (Valencia, CA) that were pre-coated with 5 nm Cr – 50 nm Au and AZ1600 positive photoresist. Sensing electrodes were patterned using standard contact lithography and etched using Au and Cr wet etchants followed by removal of the positive photoresist etchant mask. We spin-coated a negative photoresist SU-8 2002 (5000 rpm, 30 s) to create the aperture layer, and is patterned using contact lithography to create apertures 5 μm in diameter. Shipley 1811 positive photoresist was spun on the surface and patterned to create the plasma etch well layer. Chips were diced in house using a standard glass cutter. Fabrication of NMEs on the surface was done by electroplating in a solution of 20 mM HAuCl_4 and 0.5 M HCl at a constant potential of 0 mV for 90 s. A fine nanostructured Pd coating was electroplated by using a solution of 5 mM PdCl_2 and 0.5 M HClO_4 at a constant potential of -250 mV for 10 s.

E. Synthesis and purification of peptide nucleic acid

In-house synthesis of peptide nucleic acid (PNA) probes was carried out using a Protein Technologies Prelude peptide synthesizer. The following probe sequences specific to mRNA targets were utilized for detection: $\text{NH}_2\text{-Cys-Gly-Asp-ATC TGC TCT GTG GTG TAG TT-Asp-CONH}_2$ (*E. coli*), $\text{NH}_2\text{-Cys-Gly-Asp-CCC GGG GAT TTC ACA TCC AAC TT-Asp-CONH}_2$ (*P. aerugin.*), $\text{NH}_2\text{-Cys-Gly-Asp-CGA CAC CCG AAA GCG CC TTT-Asp-CONH}_2$ (*E. faecalis.*) and $\text{NH}_2\text{-Cys-Gly-Asp-CCA CAC ATC TTA TCA CCA AC-Asp-CONH}_2$ (*S. aureus*). All probes were stringently purified by reverse phase high performance liquid chromatography. Probe sequences were quantified by measuring absorbance at 260 nm with a NanoDrop and extinction coefficients were calculated from <http://www.panagene.com>

F. Bacterial samples and lysis

Escherichia coli was acquired from Invitrogen (18265-017). *E. coli* was grown in LB-Broth medium in an incubating shaker at 37 °C. After growth to the desired population the growth media was replaced with 1 \times PBS. Total RNA was extracted utilizing an Invitrogen Purelink Total RNA Extraction Kit (12183020) and quantified with the NanoDrop. Lysis of bacteria was performed utilizing a Claremont BioSolutions OmniLyse rapid cell lysis kit. Human urine samples were obtained from Bioreclamation (Westbury, NY) and were spiked with *E. coli* prior to lysis.

G. Electrochemical measurements

Electrochemical measurements were performed using a BASi EC Epsilon potentiostat in a standard 3-electrode configuration with a Ag/AgCl reference and Pt counter electrode. Acid etch scans were performed in 50 mM H_2SO_4 in H_2O . Electrocatalytic solutions contained 10 μM $\text{Ru}(\text{NH}_3)_6^{3+}$ and 4 mM $\text{Fe}(\text{CN})_6^{3-}$ in a 0.1 \times PBS buffer solution. Electrocatalytic solutions were purged with N_2 gas for 5 min prior to

electrochemical scans. Differential pulse voltammetry (DPV) was utilized to scan before and after hybridization signals.

H. Functionalization and hybridization protocol

Electrodes were functionalized with 100 nM of the designated probe and 900 nM mercaptohexanol for 30 min at room temperature. Chips were washed 2×5 min with $0.1 \times$ PBS buffer after probe deposition and sample hybridization. After washing DPV measurements were performed following probe deposition and sample hybridization in the above electrocatalytic solution. Chips were hybridized with synthetic DNA, *E. coli* total RNA, *E. coli* lysate or *E. coli* urine lysate samples for 30 min at 37 °C.

Results and discussion

A. Baseline performance of sensors fabricated on silicon

Silicon is a widely used material for photolithographic patterning and the development of high-performance devices. The ability to print multiple chips on a silicon wafer that can then be segmented into individual devices allows highly parallelized fabrication, and the ability to access this material in a form that is very flat at the nanoscale allows the generation of very intricate circuits.

Our devices are generated with a set of gold leads first being adhered and patterned onto silicon, with a passivation layer of silicon oxide or nitride then being introduced as a dielectric (Fig. 1). Apertures with diameters of ~ 5 microns are then introduced on the tips of the leads, and it is in these openings that the electrodeposition of gold is catalyzed by an applied potential. The plated metal fills the aperture, and then forms needles that grow anisotropically. The resultant structures can be characterized by SEM and optical microscopy. Electrochemical analysis can also be useful to analyze the integrity of the gold plated within the microstructure. Scanning a sensor in 50 mM H_2SO_4 produces a characteristic cyclic voltammogram that features the production of gold oxide at $\sim +1.2$ V and its removal at $+0.8$ V vs. Ag/AgCl (Fig. 1D)

Nanostructured microelectrodes produced using these chips have been studied previously,^{21–23} and shown to be effective in the specific detection of nucleic acids at femtomolar levels, even when present in unpurified crude lysates. Nucleic acid probes that are designed to be complementary of a gene of interest are designed, synthesized, and attached to the sensors *via* a thiolate linker similar as described previously.^{21,30} The reporter system used for readout leverages the electrostatic attraction between anionic nucleic acids analytes and a cationic electron acceptor $\text{Ru}(\text{NH}_3)_6^{3+}$ to generate an electrochemical response.³¹ This response is amplified with the inclusion of $\text{Fe}(\text{CN})_6^{3-}$, a more easily reduced anionic electron acceptor that efficiently reoxidizes Ru(II) and allows it to be available for further redox cycles (Fig. 1E). This reporter system allows ultrasensitive detection of nucleic acids without the need for enzymatic amplification. Fig. 1F shows representative data obtained when these sensors are exposed to solutions containing either 1 fM of a complementary sequence, or 100 nM of a non-complementary sequence. A large positive current

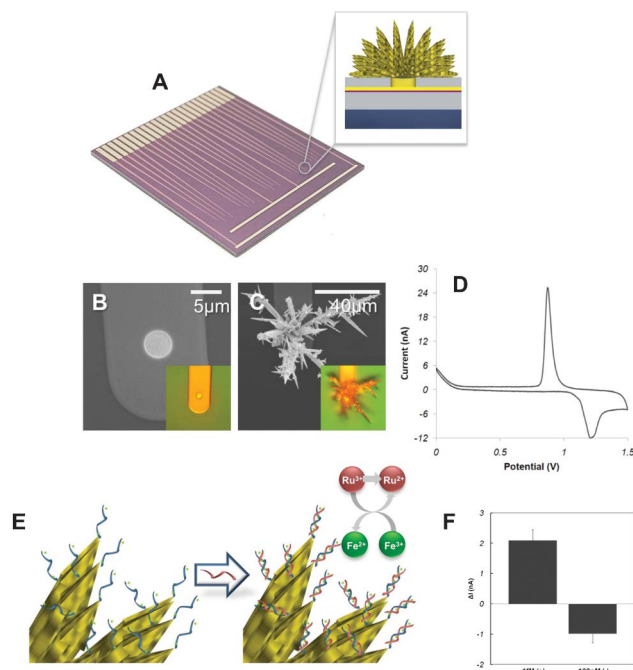


Fig. 1 Silicon-based NME characterization. (A) Silicon-based NME sensor chip. (B&C) SEM and optical image of aperture before (B) and after (C) HAuCl_4 plating. (A) Inset cross section schematic from bottom to top; Si wafer base, thermal SiO_2 , Ti-Au electrode, SiO_2 insulating layer with aperture and electroplated NME. (D) Acid scan of typical Si NME in 50 mM H_2SO_4 . (E) Electrochemical nucleic acid detection scheme PNA probe deposition and pre-scan (left), sample hybridized and post-scan (right). (F) Electrochemical current changes observed when sensors coated with the same probe were incubated with 1 fM complementary (+) and 100 nM non-complementary (–) DNA sequences.

change is observed with the complement, while a negative current change is observed with a non-complement. The latter effect is expected to arise because non-specifically bound probe is washed away during hybridization and lowers the overall background signal.

B. Testing of printed circuit board as a substrate for sensor deposition

While impressive performance and femtomolar detection limits were achieved with electrodeposited gold sensors fabricated on silicon, it was unclear whether such a refined material was required. We hypothesize that the impressive performance of Si based sensors is dependent only on the morphology and composition of the electrodeposited sensor itself and not on the base substrate. Given the need to keep materials costs at a minimum for eventual clinical use of the sensor system, an exploration of other substrates was merited. Printed circuit boards, which can be rapidly fabricated without the need for expensive masks, were an excellent candidate for testing. Electrode arrays of recessed apertures could be straightforwardly and rapidly produced, and with an inherent cost much lower than silicon.

Printed circuit board based sensor chips were made that featured apertures created in the soldermask layer that could be used to template NME growth. In order to prevent corrosion

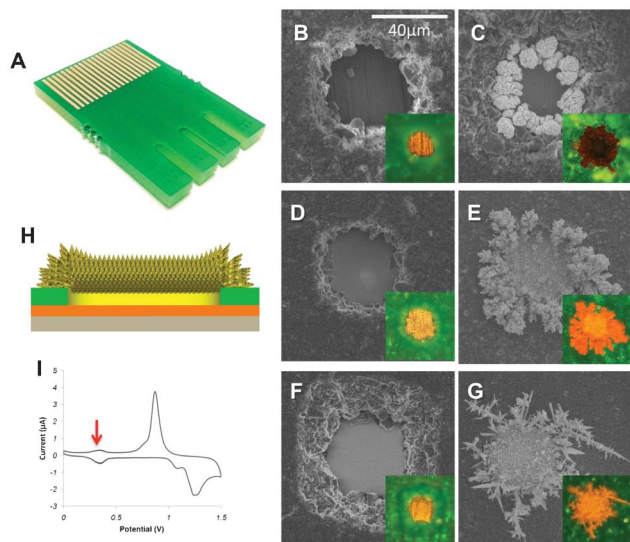


Fig. 2 PCB-based NME characterization. (A) Image of PCB NME sensor chip. (B) SEM and optical image of aperture before plating. Immersing in HAuCl_4 causes corrosion of copper layer (C). To prevent corrosion, PCBs were plated first with NiSO_4 (D) or with AuSO_3 (F) and subsequently plated with HAuCl_4 shown respectively in (E) and (G). Cross section schematic (H) from bottom to top; FR-4 PCB fiberglass base, Cu electrode layer, soldermask insulating layer with aperture filled by plating with (D) or (F), electroplated NME. (I) Acid scan of typical PCB NME from (G) in 50 mM H_2SO_4 .

of Cu during electroplating (Fig. 2C), it was necessary to produce an initial protection layer of NiSO_4 (Fig. 2D) or AuSO_3 (Fig. 2F). To create extruded electrodes for electrochemical sensing the protection layer was followed by electroplating $\text{Au}(\text{OH})_2$ (Fig. 2E) or HAuCl_4 (Fig. 2G). Electrodes fabricated in this fashion exhibit increased growth at the aperture edges as compared with the recessed centre. This is a direct result of a loss in aperture resolution ($40\ \mu\text{m}$), compared to Si ($5\ \mu\text{m}$) and the thickness of soldermask layer ($\sim 50\ \mu\text{m}$) compared the Si passivating layer ($<1\ \mu\text{m}$). The recessed center of the aperture would experience much slower diffusion of the plating reagents, and this would worsen as the edges of the aperture are plated.

Electrochemical analysis was performed to interrogate the integrity of the gold plated in PCB NMEs (Fig. 2I). The characteristic gold oxidative peak at $\sim 1.2\ \text{V}$ and reductive peak at $\sim 0.8\ \text{V}$ vs. Ag/AgCl is observed similar to Si. However, an auxiliary peak appears at $\sim 0.3\ \text{V}$ which is likely due to Cu impurities from the underlying Cu layer given the ability of this element to migrate through Au.

The performance of electrochemical sensors generated with PCB as a base was poor and inconsistent when compared to Si NMEs. When the DNA detection experiment described above was used to benchmark performance, large background currents were observed leading to poor signal to noise, and the Cu impurities in the Au NMEs made the quantitation of signals due to DNA binding difficult to monitor (data not shown).

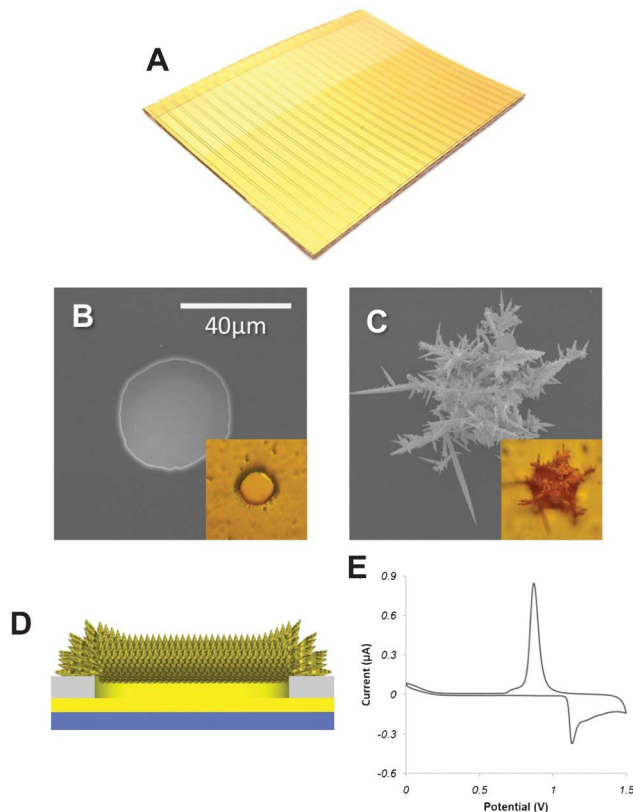


Fig. 3 Plastic-supported NME characterization. (A) Image of plastic NME sensor chip. (B&C) SEM and optical image of aperture before (B) and after plating (C) in HAuCl_4 . (D) Cross-section schematic from bottom to top; plastic base, Au electrode layer, SU-8 insulating layer with aperture, electroplated NME. (E) Acid scan of typical plastic-supported NME in 50 mM H_2SO_4 .

C. Testing of plastic as a substrate for sensor deposition

Given the incompatibility of metal-containing materials for NME fabrication, we focused on more inert substrates that might be better suited for producing robust structures. We tested fluorinated ethylene polymer (FEP) a common flexible printed circuit material as a substrate for NME growth. A printed Au ink was used to generate the Au leads, and an insulating SU-8 aperture layer was added using traditional cleanroom techniques. The flexibility of FEP posed a challenge, as it was difficult to process reliably, since both spin coating SU-8 and contact mask lithography is difficult and unreliable, and produces apertures with poor resolution that can't be made smaller than $40\ \mu\text{m}$.

Electroplating of the FEP-based NMEs (Fig. 3C) was straightforward and used the same plating method as with Si NMEs. The structures obtained again featured recessed sections in the center of the aperture, indicating that this effect does arise because of the large size of the aperture. Electrochemical analysis was again performed to interrogate the integrity of the gold electroplated in FEP-based NMEs (Fig. 3E). The cyclic voltammograms of these structures did not contain any peaks except those characteristic of gold. However, performance of electrochemical DNA sensing with the FEP-based NMEs was poor ($\sim 100\ \text{nM}$ limit of detection)

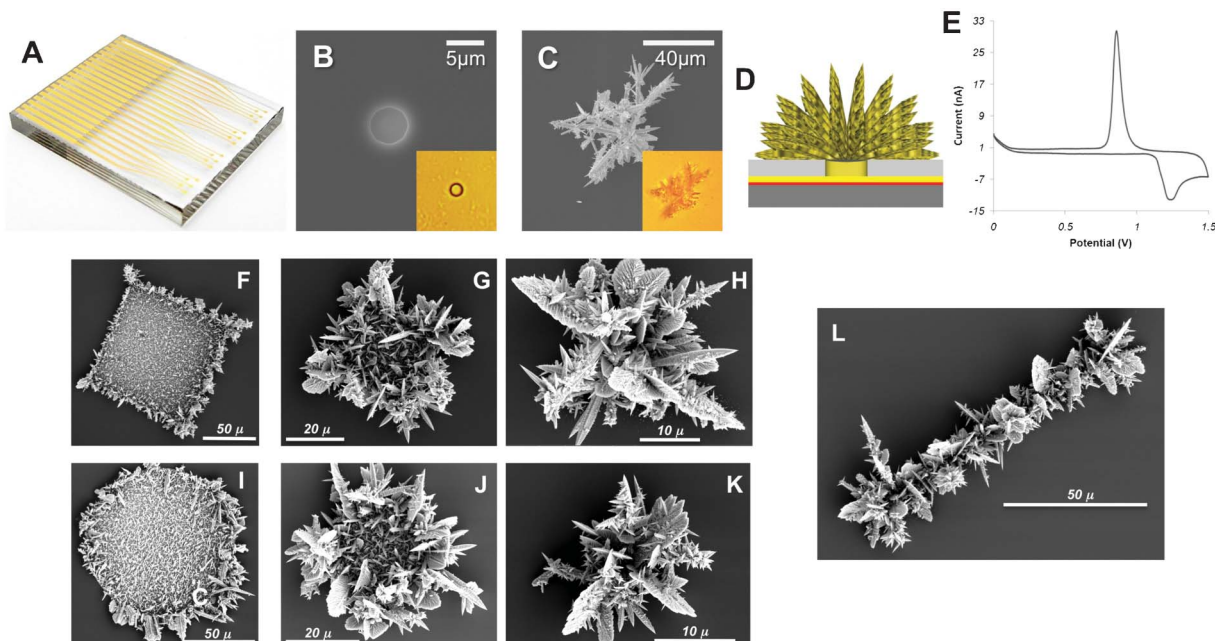


Fig. 4 Glass-supported NME characterization. (A) Image of a glass NME sensor chip. (B&C) SEM and optical image of aperture before (B) and after plating (C) in HAuCl_4 . (D) Cross section schematic from bottom to top; glass base, Cr–Au electrode layer, SU-8 insulating layer with aperture, electroplated NME. (E) Acid scan of typical glass NME in 50 mM H_2SO_4 . (F, G, H) Electrodeposition within 100, 25, and 5 micron square apertures, respectively. (I, J, K) Electrodeposition within 100, 25, and 5 micron circular apertures, respectively. (L) Electrodeposition in an aperture 100 microns by 5 microns.

and inconsistent as compared with Si NMEs. The inability to generate a structure that features the same verticality of the silicon-based NMEs likely affects sensitivity, and limits the participation of the entire structure in productive collisions with target molecules.

D. Testing of glass as a substrate for sensor deposition

We also tested borosilicate glass as potential substrate to evaluate whether it possessed better features for NME growth. The rigidity and inertness of this material makes it a good substitute for silicon, but it is much more cost-effective alternative. Glass-based NME structures were fabricated on the surface of plain borosilicate glass (Fig. 4). Glass slides were coated with an Au gold layer and positive photoresist, and SU-8 and contact mask lithography were used to generate aperture patterns. The aperture sizes generated were comparable to those obtained with silicon (Fig. 4B) and were highly reproducible.

Electroplating of glass-based NMEs (Fig. 4C) was performed using the same protocol needed to produce Si-based NMEs, and structures were produced that exhibited similar sizes and morphologies. Electrochemistry was again used to investigate the integrity of the Au electroplated in glass NMEs (Fig. 4E), and the expected scans were obtained reflecting pure Au NMEs.

We also investigated the role of aperture size and shape on the morphology of glass NME structures (Fig. 4F–4L). We observed that structures with larger aperture size 25 μm or greater exhibit edge effects and recessed interiors, regardless if the aperture is square or circular (Fig. 4F, 4G, 4I, 4J). As aperture size is decreased to 5 μm (Fig. 4 H,K), edge effects are

no longer an issue and structures protrude in a more uniform fashion without apparent recessed areas. Restriction to 5 μm in one-dimension only (Fig. 4L) is sufficient to eliminate the edge effect, where electrodes protrude in a uniform fashion along the lateral direction.

E. Validation of clinically-relevant sensitivity and specificity using glass chips

Given that glass appeared to support the growth of structures that were physically and electrochemically indistinguishable from those made on silicon, we evaluated the performance of the NMEs when challenged with synthetic oligonucleotides, and crude *E. coli* lysates in buffer and urine. These experiments were performed with different types of sensors that target different bacterial organisms: *E. coli*, *E. faecalis*, *S. aureus*, or *P. aeruginosa*. In any given trial, *E. coli* sensors were tested alongside two types of non-target sensors in order to assess specificity (Fig. 5). Excellent sensitivity and specificity was observed, indicating that the glass-based sensors are comparable to those originally generated on silicon.

Conclusions

Here we have investigated various materials that possess desirable manufacturing qualities including low-cost and quick design to prototype cycles. Printed circuit board is one of the lowest cost materials, with well-established quick and cheap manufacturability. However, issues arose with Cu compatibility and large background currents due to loss in aperture resolution, which led to poor assay performance. A

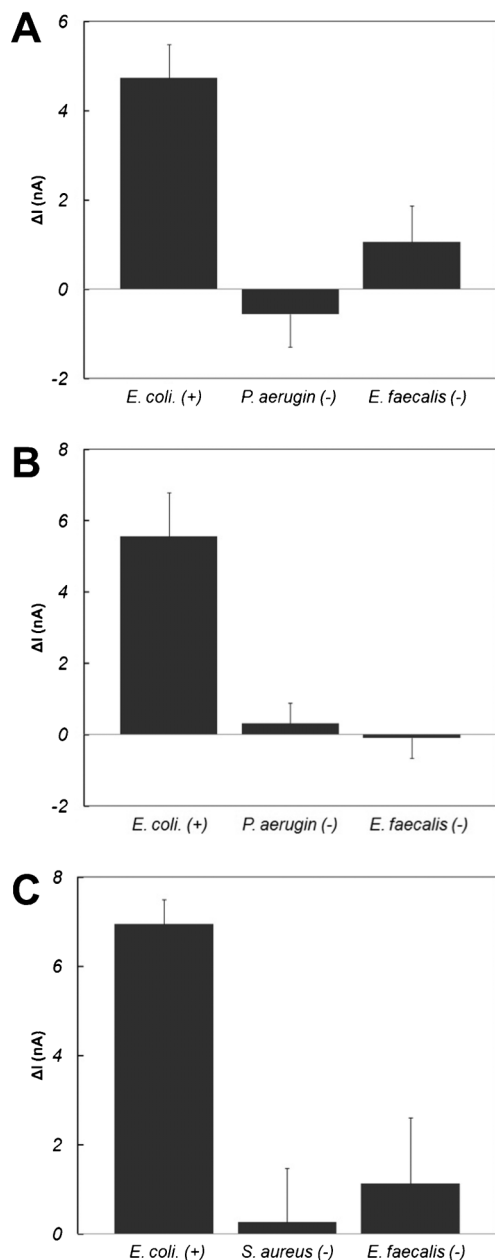


Fig. 5 Glass-based NME assay validation. All chips were coated with specific pathogen probes and challenged with (A) total *E. coli* RNA extract ($1 \text{ ng } \mu\text{L}^{-1}$) (B) *E. coli* lysate ($100 \text{ cfu } \mu\text{L}^{-1}$) and (C) urine samples spiked with $100 \text{ cfu } \mu\text{L}^{-1}$ *E. coli* and subsequently lysed.

plastic was also tested that appeared to be an ideal low cost material, but due to the flexible nature of the material lithographic processing is difficult and produces apertures with low resolution, resulting in large background currents and poor electrochemical assay performance.

Our investigation of standard borosilicate glass as a substrate for NME growth revealed that this is the best substrate for NME growth. We found that glass has sufficient rigidity and flatness for lithographic techniques required for small aperture sizes, yet it is widely available and low-cost. We

found that aperture size is the main factor in eliminating predominate edge growth effects, which would cause recessed electrodes that are undesirable for electrochemical sensing. These results are generally applicable to the electrodeposition of any type of microscale structured template for growth.

Acknowledgements

This research was sponsored by the Defense Advanced Research Projects Agency through the Autonomous Diagnostics to Enable Prevention and Therapeutics: Diagnostics on Demand-Point-of-Care (ADEPT:DxOD-POC) program and the Ontario Research Fund (Research Excellence Program).

Notes and references

- 1 A. L. Washburn and R. C. Bailey, *Analyst*, 2011, **136**, 227–236.
- 2 K. Balasubramanian, *Biosens. Bioelectron.*, 2011, **26**, 1195–1204.
- 3 D. R. Walt, *Science*, 2005, **308**, 217–219.
- 4 K. B. Cederquist and S. O. Kelley, *Curr. Opin. Chem. Biol.*, 2012, **16**, 415–421.
- 5 N. L. Rosi and C. A. Mirkin, *Chem. Rev.*, 2005, **105**(4), 1547–1562.
- 6 T. Hianik and J. Wang, *Electroanalysis*, 2009, **21**, 1223–1235.
- 7 D. A. Giljohann, D. S. Seferos, W. L. Daniel, M. D. Massich, P. C. Patel and C. A. Mirkin, *Angew. Chem., Int. Ed.*, 2010, **49**, 3280–3294.
- 8 G. Yu and C. M. Lieber, *Pure Appl. Chem.*, 2010, **82**, 2295–2314.
- 9 K. E. Sapsford, J. Francis, S. Sun, Y. Kostov and A. Rasooly, *Anal. Bioanal. Chem.*, 2009, **394**, 499–505.
- 10 C. H. Park, J. P. Kim, S. W. Lee, N. L. Jeon, P. J. Yoo and S. J. Sim, *Adv. Funct. Mater.*, 2009, **19**, 3703–3710.
- 11 X. Duan, Y. Li, N. K. Rajan, D. A. Routenberg, Y. Modis and M. A. Reed, *Nat. Nanotechnol.*, 2012, **7**, 401–7.
- 12 T. M. Alligant, E. G. Nettleton and R. M. Crooks, *Lab Chip*, 2013, **13**, 349–54.
- 13 J. D. Slinker, N. B. Muren, A. A. Gorodetsky and J. K. Barton, *J. Am. Chem. Soc.*, 2010, **132**, 2769–2774.
- 14 Y. Xiao, A. A. Lubin, B. R. Baker, K. W. Plaxco and A. J. Heeger, *Proc. Natl. Acad. Sci. U. S. A.*, 2006, **103**, 16677–80.
- 15 R. Malhotra, V. Patel, J. P. Vaqu e, J. S. Gutkind and J. F. Rusling, *Anal. Chem.*, 2010, **82**, 3118–23.
- 16 J. Das and S. O. Kelley, *Anal. Chem.*, 2011, **83**, 1167–72.
- 17 J. Das, K. Cederquist, A. A. Zaragoza and P. E. Lee, *Nat. Chem.*, 2012, **4**, 642–8.
- 18 T. M. Squires, R. J. Messinger and S. R. Manalis, *Nat. Biotechnol.*, 2008, **26**, 417–426.
- 19 P. E. Sheehan and L. J. Whitman, *Nano Lett.*, 2005, **5**, 803–807.
- 20 P. R. Nair and M. A. Alam, *Nano Lett.*, 2008, **8**, 1281–1285.
- 21 L. Soleymani, Z. Fang, B. Lam, X. Bin, E. Vasilyeva, A. J. Ross, E. H. Sargent and S. O. Kelley, *ACS Nano*, 2011, **5**, 3360–3366.

- 22 L. Soleymani, Z. Fang, E. H. Sargent and S. O. Kelley, *Nat. Nanotechnol.*, 2009, **4**, 844–848.
- 23 X. Bin, E. H. Sargent and S. O. Kelley, *Anal. Chem.*, 2010, **82**, 5928–5931.
- 24 B. J. Plowman, S. K. Bhargava and A. P. O'Mullane, *Analyst*, 2011, **136**, 5107–5119.
- 25 S. E. Brunner, K. B. Cederquist and C. D. Keating, *Nanomedicine*, 2007, **2**, 695–710.
- 26 D. Bera, S. C. Kuiry and S. Seal, *JOM*, 2004, **56**, 49–53.
- 27 D. Bera, S. C. Kuiry, S. Patil and S. Seal, *Appl. Phys. Lett.*, 2003, **82**, 3089–3092.
- 28 G. Fasol and K. Runge, *Appl. Phys. Lett.*, 1997, **70**, 2467–2468.
- 29 D. Wang, W. L. Zhou, B. F. McCaughy, J. E. Hampsey, X. Ji, Y.-B. Jiang, H. Xu, J. Tang, R. H. Schmehl, C. O'Connor, C. J. Brinker and Y. Lu, *Adv. Mater.*, 2003, **15**, 130–133.
- 30 E. Vasilyeva, *et al.*, *Angew. Chem., Int. Ed.*, 2011, **50**, 4137–41.
- 31 M. A. Lapierre, M. O'Keefe, B. J. Taft and S.O. Kelley, *Anal. Chem.*, 2003, **75**, 6327–6333.